Composites Part B 87 (2016) 350–356

Contents lists available at ScienceDirect

Composites Part B

journal homepage: www.elsevier.com/locate/compositesb

Effect of the morphology of thermally reduced graphite oxide on the mechanical and electrical properties of natural rubber nanocomposites

Héctor Aguilar-Bolados [a, *], Miguel A. Lopez-Manchado [b], Justo Brasero [b], F. Avilés [c], Mehrdad Yazdani-Pedram [a]

[a] Faculty of Chemical and Pharmaceutical Sciences, Universidad de Chile, S. Livingstone 1007, Santiago, Chile
[b] Instituto de Ciencia y Tecnología de Polímeros, ICTP-CSIC, Juan de la Cierva, 3, 28006 Madrid, Spain
[c] Centro de Investigación Científica de Yucatán, Unidad de Materiales, Calle 43, No. 130 Col. Chuburná de Hidalgo, 97200 Mérida, Yucatán, Mexico

ARTICLE INFO

Article history:
Received 25 April 2015
Received in revised form
24 August 2015
Accepted 27 August 2015
Available online 5 September 2015

Keywords:
A. Polymer–matrix composites (PMCs)
B. Electrical properties
B. Mechanical properties
D. Electron microscopy

ABSTRACT

Graphene materials often are obtained through thermal reduction of graphite oxide. This is due to the fact that other synthesis methods are more difficult and generally render lower yield. The structure and morphology of these graphene materials could affect their performance in different applications. Herein, thermally reduced graphite oxide (TRGO) was obtained from thermal reduction of graphite oxide prepared by using the methods reported by Brodie and Hummers. The oxidation method greatly affects the structure and morphology of the resulting TRGO. TRGO obtained by the Brodie's method generates a morphology comprised of rather exfoliated galleries while that obtained by the Hummers method presents randomly distributed sheets. The influence of structural differences on the dispersion of TRGOs in natural rubber latex (NR) and on the resulting mechanical and electrical properties of the TRGO/NR nanocomposites is studied. The TRGO prepared by the Brodie's method (TRGO-B) showed a more homogeneous dispersion in the polymer–matrix, rendering enhanced mechanical and electrical properties of their nanocomposites. TRGO-B/NR nanocomposites showed higher electrical conductivity, which is attributed to the formation of an electrically conducting filler network through the polymer–matrix. This is consequence of the morphology presented by TRGO produced by the Brodie's method.

1. Introduction

Graphite is a carbon allotrope with planar layered structure widely available in nature [1]. An isolated layer of graphite is known as graphene. In graphene the carbon atoms are bonded by sp^2 hybridization and the single atomic layer character renders its outstanding physical properties [2]. Although an isolated layer of graphene is normally not found in nature, the group of Novoselov and Geim [3] are well known for isolating stable graphene. The micromechanical exfoliation used by Novoselov et al. is not feasible for large scale preparation of graphene. Therefore, other methods to produce graphene or a few layers of exfoliated graphene materials have been proposed [3,4]. The method known as "top-down" comprises in the production of graphene materials from graphite. Examples of "top-down" methods are ultrasound treatment of graphite in suspension [4] and the exfoliation of graphite oxide by thermal or chemical reduction [5]. The exfoliation process of graphite oxide through a quick thermal expansion is probably the most used method owing to facility, viability and high yield [6]. The graphite oxide frequently used for obtaining graphene materials are those obtained by oxidation of graphite by methods reported by Brodie [7], Staudenmaier [8] or Hummers and Offerman [9].

Brodie [7] proposes the use of potassium chlorate ($KClO_3$) and fuming nitric acid (HNO_3), without formation of perchlorates, where the chloric acid ($HClO_3$) is probably the main oxidizing species [10]. The Hummers' method [9] consists in the use of potassium permanganate ($KMnO_4$), sodium nitrate ($NaNO_3$) and concentrated sulfuric acid (H_2SO_4). The oxidizing species in the Hummers' method could correspond to manganese heptoxide (Mn_2O_7) [11]. Botas et al. [12] studied the thermal reduction of graphite oxide prepared by the Brodie's (GO-B) and Hummers' (GO-H) methods, demonstrating that GO-H presents higher oxygen

* Corresponding author. Tel.: +56 2 2978 2855.
E-mail address: haguilar@ciq.uchile.cl (H. Aguilar-Bolados).

http://dx.doi.org/10.1016/j.compositesb.2015.08.079
1359-8368/

content than GO-B. However, thermal reduction of GO-H and GO-B upon 1000 °C produced TRGO-H with lower oxygen content than TRGO-B.

The excellent intrinsic properties of graphene [13] are probably the main reason for the huge interest of using graphene materials as mechanical reinforcement and/or electro-conducting filler for polymer matrices [14]. However, the difficulty to produce graphene monolayer and to prevent such an individual layers from recombining within the polymer–matrix has induced researchers to employ graphene materials obtained either by chemical (CRGO) or thermal (TRGO) reduction of graphite oxides as fillers for polymer matrices [15–23]. Different authors have reported the use of natural rubber (NR) as matrix for the preparation of electrically conducting elastomeric nanocomposites by using TRGOs or CRGOs as fillers [24–31]. Some of these reports have employed natural rubber latex at some stage of the nanocomposite preparation [26–33]. Zhan et al. [26] reported the homogeneous dispersion of CRGO in NR obtaining nanocomposites with excellent mechanical properties. These nanocomposites were prepared by coagulation of NR latex in presence of CRGO, mixed in a two roll mill and then vulcanized. Similar works were developed by Potts et al. [28,29], where they observed that processing of coagulated NR containing TRGO in a two roll mill yields better mechanical and electrical properties compared with the properties of those prepared by the direct addition of TRGO to NR during two roll milling. Aguilar-Bolados et al. [31] reported a simple and more efficient method for the preparation of TRGO/NR nanocomposites by the addition of aqueous suspension of TRGO and surfactant to prevulcanized natural rubber latex. The use of prevulcanized natural rubber latex allows the production of homogeneous films with improved mechanical and electrical properties, without the need of post-processing stages.

In spite of these research progresses, there is no clear understanding of how the method of synthesis of TRGO affects the electrical and mechanical properties of nanocomposites. Therefore, this work reports on the synthesis of graphite oxides produced by using the methods reported by Brodie [7] and Hummers [9]. The graphite oxides are subsequently thermally reduced to obtain TRGO for investigating their effect on the mechanical and electrical properties of NR composites. The aim of this work is to study the effect of the morphology of both TRGO on the mechanical and electrical properties of TRGO/NR nanocomposites prepared by latex technology.

2. Materials and methods

2.1. Materials

Commercial natural graphite powder supplied by Sigma–Aldrich was used for the preparation of graphite oxides. The carbon content was 99.9 wt.%. Fuming nitric acid (≥99.5%), potassium chlorate (≥99%), sulfuric acid (98%), sodium nitrate (≥99.5%) and potassium permanganate (≥99%) were from Sigma–Aldrich and were used as received.

2.2. Synthesis of graphite oxide

2.2.1. Brodie's method

5 g of graphite were added to 100 ml of fuming nitric acid into a flask with a cooling jacket and cooled to 0 °C in a cryostat bath. Next, 40 g of potassium chlorate was slowly added for 1 h and the reaction mixture was stirred for 21 h at 0 °C. Once the reaction finished, the suspension was centrifuged (3700 rpm for 30 min), washed with distilled water and vacuum filtered until the pH of the filtrate was neutral.

2.2.2. Hummers' method

44 ml of sulfuric acid, 1 g of sodium nitrate and 2 g of graphite were added to a refrigerated reactor and cooled down to 0 °C. Next, 6 g of potassium permanganate was slowly added to keep the reaction temperature below 20 °C. This mixture was then heated to 37 °C under stirring for 3 h, followed by the addition of 88 ml of distilled water. Then, 3% H_2O_2 was slowly added until a color change was observed. The mixture was then washed with distilled water and vacuum filtered until the pH was neutral. Finally, the suspension was dried at 70 °C.

2.3. Synthesis of thermally reduced graphite oxide

The thermal exfoliation and reduction of GO-B and GO-H for the preparation of thermally reduced graphite oxide (TRGO) was performed in a Carbolite® TZF 12/65/550 horizontal furnace tube at 1000 °C under an argon atmosphere (500 ml/min). 0.3 g of GO was introduced into the furnace and heated first to 200 °C at a rate of 20 °C/min and then at 10 °C/min up to 1000 °C, maintaining this temperature for 1 h. The corresponding samples obtained were labeled as TRGO-B and TRGO-H, where the last letter indicates the oxidation method used.

2.4. Preparation of TRGO/NR nanocomposites

For the preparation of TRGO/NR nanocomposites, a colloidal suspension of TRGO in an aqueous solution of 22.5 mM of dodecyltrimethylammonium bromide (DTAB) from Merck was prepared and subjected to ultrasound for 30 min at room temperature. This suspension was added to prevulcanized natural rubber latex from Química Miralles S.A. with 49.62 wt.% rubber content. This suspension was immediately poured to a Petri dish and then dried at 70 °C to form a film. The diameter and thickness of the films were around 15 cm and 200 μm, respectively. Specimens for mechanical and electrical testing were obtained from these films. The content of TRGO in the nanocomposites was 2, 3 and 4 wt.% with respect to the NR. Each of these nanocomposites contained 4.6, 6.9 and 9.3 wt.% of DTAB as surfactant with respect to the NR.

2.5. Characterization of TRGOs and TRGO/NR nanocomposites

TRGOs were characterized by Raman spectroscopy using a Renishaw Invia Confocal Raman Microscope equipped with an argon laser of 514.5 nm excitation wavelength and 0.02 cm^{-1} resolution. The spectra were recorded from 750 to 3500 cm^{-1}. To determine the interlayer distance of TRGO, X-ray diffraction (XRD) analysis of the powdered samples was performed using a Bruker D8 Advance diffractometer with a CuKα radiation source, wavelength $\lambda = 0.154$ nm and a power supply of 40 kV and 40 mA. The incidence angle (2θ) was varied between 1° and 60° and the scan rate was 0.02°/s. The interlaminar sheet distance was obtained from the (002) reflection of the XRD patterns of the TRGOs. The morphology of the TRGOs was studied using a scanning electron microscope (SEM) Vega 3 Tescan.

Tensile stress–strain properties of vulcanized NR latex and its nanocomposites were measured in an Instron dynamometer model 3366 at 25 °C using a cross-head speed of 500 mm/min and following the ASTM D412 specification [34]. Rectangular-shaped specimens were cut from the vulcanized films. Five specimens of each material were tested.

Broadband dielectric spectroscopy (BDS) measurements were performed in a Novocontrol ALPHA high resolution dielectric analyzer. Vulcanized film disc-shaped samples were mounted in the dielectric cell between two parallel gold-plated electrodes. The film thickness (nominally 100 mm) was considered as the distance

between electrodes and measured using a micrometer gauge. The dielectric response of each sample was assessed by measuring the complex permittivity, $\varepsilon^*(\omega) = \varepsilon'(\omega) + j\varepsilon''(\omega)$ where $j^2 = -1$, as a function of the frequency (ω), over a frequency range of 10^{-1} to 10^7 Hz at 25 °C. The amplitude of the alternating electric voltage applied to the samples was 1 V. The AC conductivity ($\sigma(\omega)$) was measured in the same conditions as ε^*. In a conducting composite, the conductivity is composed of two terms, i.e. $\sigma(\omega) = \sigma_{dc} + A\omega^x$, where σ_{dc} is the direct current conductivity, A is a constant and x is an exponent which describes the frequency (ω) dependence of $\sigma(\omega)$. The term σ_{dc} appears as a plateau at low frequencies in the experiments and is obtained by extrapolating the broadband AC conductivity to 10^{-1} Hz, when such a plateau is reached.

3. Results

3.1. Characterization of graphene materials

Fig. 1 shows XRD patterns of natural graphite (NG) and graphite oxides prepared by two oxidation methods, viz. Brodie's one (GO-B) and Hummers' one (GO-H). NG exhibits a strong crystalline peak at 26.2° which corresponds to the d_{002} diffraction plane. This peak is shifted towards lower angles when NG is oxidized, and the interlayer distance increases from 0.34 nm for NG to 0.60 nm and 0.84 nm for GO-B and GO-H, respectively. This increase in the interlayer distance is the result of the presence of oxygenated functional groups. It has been reported that the increase of interlayer distance in graphite through an oxidation process is proportional to the oxidation degree of graphite [35]. Therefore, the larger interlayer distance of GO-H evidences a more extensive oxidation. When the GOs are thermally reduced, the diffraction peak related to the d_{002} plane disappears in both TRGO-B and TRGO-H. This suggests that a partial elimination of oxygen-containing groups occurs from the graphitic structure during the thermal reduction process, which promotes the exfoliation of TRGO layers [36].

Fig. 2 shows the Raman spectra of natural graphite, GO-B, GO-H, TRGO-B and TRGO-H. NG displays a weak band at 1348 cm^{-1} attributed to the so called *D* band, which is associated to "defects" or functionalities, and a prominent *G* band at 1573 cm^{-1} corresponding to the first-order scattering of the E_{2g} phonon mode of sp^2 carbon atoms [37]. The *D* band of both TRGOs is more intense and the *D* and *G* bands of TRGO-B and TRGO-H are significantly broadened and shifted with respect to the corresponding *D* and *G* bands of graphite. The increase in intensity of the *D* band suggests

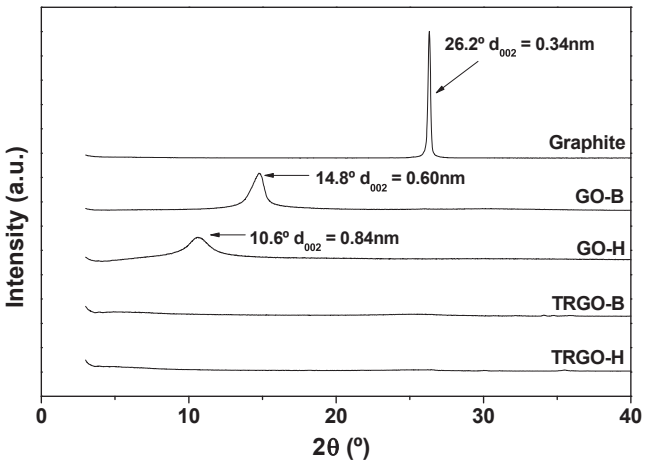

Fig. 1. X-ray diffraction patterns of natural graphite (NG), GO-B, GO-H, TRGO-B and TRGO-H.

an increase of functional groups and/or defects generated in the TRGO layers as a result of the oxidation process used [38]. Nevertheless, after reduction, a decrease of the *D* band intensity is observed with respect to those of GOs. This decrease in the intensity of the *D* band could indicate the recovering of the in-plane sp^2 domains, possibly due to the reduction process [39]. In addition, the Lorentzian fitting analysis of the *G* band of TRGO indicates the presence of a band around 1610 cm^{-1} which can be attributed to the *D′* band (Fig. 2). The *D′* band has been associated to the presence of defects in graphitic planes [38–40].

Table 1 summarizes the Raman features of the observed bands, including the position (shift), full width at half-maximum (FWHM) and the ratio of intensities of the *D* to *G* bands (I_D/I_G). Differences between the location of the *D*, *G* and *D′* bands for GO-B and GO-H could be attributed to different morphology and interlayer distance obtained by using different oxidation processes [38]. The intensity ratios of the *D* and *G* bands (I_D/I_G) have been used to describe the defect density in graphene and other carbon nanostructures [39]. GO-H exhibits the highest I_D/I_G, almost twice of that of GO-B. This suggests that GO-H contains more structural defects and probably functionalities as a result of the oxidation method used. After thermal treatment, both TRGO-B and TRGO-H have similar I_D/I_G values, much higher than that of graphite. I_D/I_G ratio indicates that both TRGOs contain structural defects and some residual oxygen functionalities [41]. The GO-H shows an important decrease of I_D/I_G after thermal treatment, which could indicate the occurrence of a partial loss of oxygen functionalities, which occurs with a recovering of sp^2 carbon lattices [12,40]. On the other hand, GO-B shows a slight increase of I_D/I_G after thermal treatment due probably to two facts i) the residual oxygen functionality [12] and ii) higher structural defects, such as a decrease of the size of a nanocrystallite and point of defects on sp^2 carbon lattices [40,42]. It has been reported that GO-H and GO-B have different profiles of thermogravimetric analysis. The maximum weight loss of GO-H occurs at 200 °C while for GO-B occurs at 250 °C [12]. This could indicate that there are differences in the kinetics of oxygen elimination. Hence, the decrease or increase of I_D/I_G ratio experimented by both GOs (GO-H or GO-B, respectively) after the thermal treatment could mainly be attributed to the behavior of oxygen elimination kinetics for both GOs, which could be further studied. These structural defects and oxygen functionalities may promote bonding between the TRGOs and the NR during the nanocomposite preparation.

Important morphological differences between the samples prepared by using different oxidation methods can be observed by SEM (Fig. 3). TRGO-B (Fig. 3a and b) exhibits small areas showing stacked galleries typical of expanded graphite, indicating a partial exfoliation of GO [12]. On the other hand, TRGO-H (Fig. 3c and d) shows randomly oriented sheets without visible sheet stacking. Botas et al. [12] showed that the partially exfoliated stacked gallery morphology of TRGO-B present higher surface area than TRGO-H. This could facilitate the adsorption of the surfactant on TRGO-B layers. The surfactant is used for stabilizing the aqueous TRGO-B suspension employed for nanocomposite preparation. Consequently, a higher dispersion of TRGO-B in the NR matrix may be expected, resulting in a better interaction between the TRGO-B particles and NR.

3.2. Morphology of TRGO/NR nanocomposites

Fig. 4 shows TEM images of different TRGO/NR nanocomposites. At the nanoscale, the TRGO-B layers (Fig. 4a and b) have a considerable larger separation among them than the TRGO-H (Fig. 4c and d), although both tend to form small aggregates at the microscale. Moreover, TRGO-B layers form an interconnected network in the

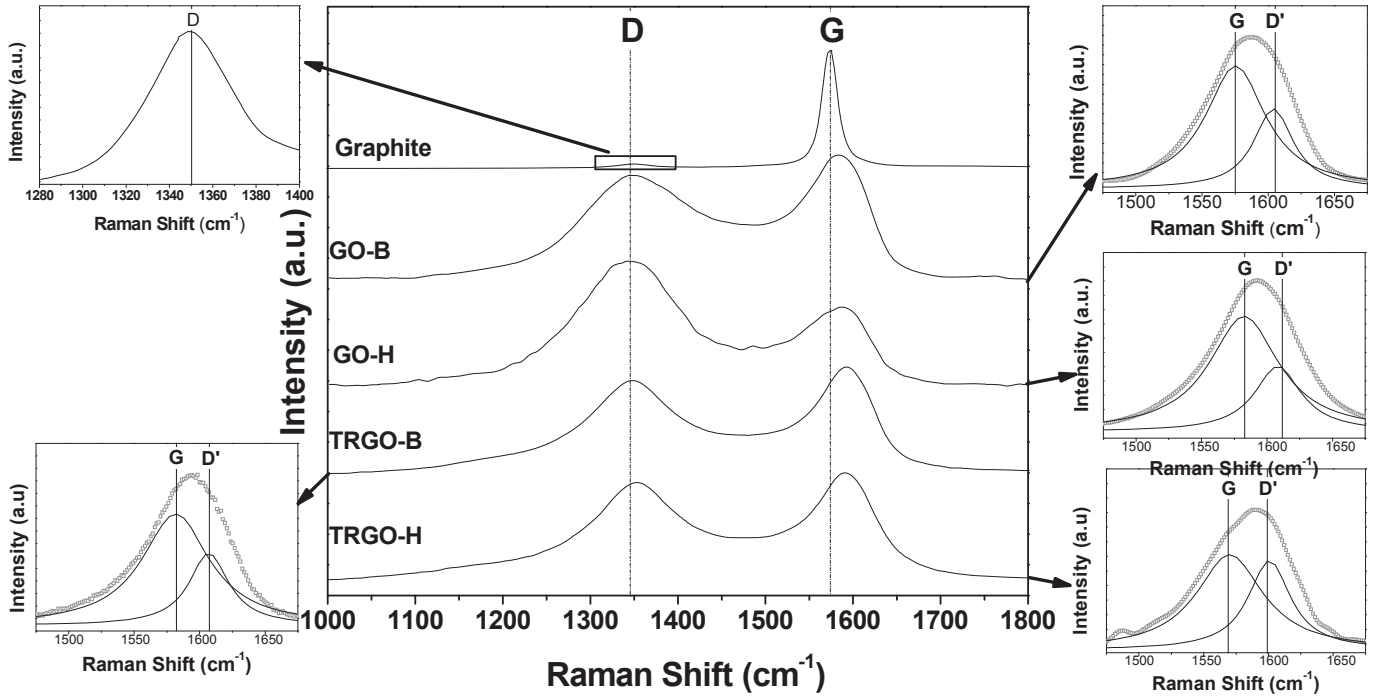

Fig. 2. Raman spectra of NG, GO-B, GO-H, TRGO-B and TRGO-H. Inset shows a close-up of the D band of graphite (top left) and examples of Lorentzian fitting analysis of the *G* band for GO-B, GO-H, TRGO-B and TGO-H.

Table 1
Raman shift, FWHM and I_D/I_G ratios for NG, TRGO-B and TRGO-H.

	Raman shift (cm^{-1})			FWHM (cm^{-1})			I_D/I_G
	D	*G*	*D′*	*D*	*G*	*D′*	
NG	1349	1573	–	44.0	19.9	–	0.06
GO-B	1361	1575	1604	73.4	55.4	36.8	0.83
GO-H	1344	1570	1601	63.0	62.7	39.6	1.61
TRGO-B	1345	1582	1607	91.9	62.7	37.1	0.89
TRGO-H	1350	1583	1608	87.7	64.9	43.8	0.92

polymer–matrix, which could be promoted by its exfoliated gallery morphology which facilitates the adsorption of the surfactant, and possibly π-electron transfer. On the other hand, the TRGO-H layers appear randomly distributed without a clear stacking pattern, presumably rendering less formation of interconnected networks.

3.3. Mechanical properties of TRGO/NR nanocomposites

Table 2 shows the tensile mechanical properties of TRGO/NR nanocomposites. The mechanical properties of natural rubber control samples containing different amounts of DTAB as surfactant are also shown in Table 2. The surfactant behaves as a plasticizer favoring the coalescence of latex particles [43], which is reflected in a decrease of stiffness, expressed as the stress at several deformations, and strength. The addition of TRGO enhances the mechanical properties of NR, especially the stiffness when TRGO-B is used as nanofiller. Improvements in the stress at 500% strain of more than twice are achieved when 2 wt.% TRGO-B is added to the NR matrix. This stiffening effect is similar to that observed for NR when other methods for the preparation of nanocomposites such as melt mixing by two roll milling of coagulated NR containing TRGO were used [29]. However, when two roll milling of coagulated NR is used, the ultimate strain of the nanocomposite is greatly sacrificed, while the reduction for the composites prepared by TRGO dispersion in prevulcanized NR latex is only minor. The improved mechanical properties observed for composites prepared by using TRGO-B with respect to those with TRGO-H could be attributed to the morphology of stacked galleries of TRGO-B with highly interconnected graphene layers, which promotes rubber-TRGO interactions. In the case of TRGO-H, the randomly oriented graphene layers with low interconnection among the layers may hinder the homogeneous dispersion in the NR matrix, causing stress concentrations.

3.4. Electrical properties of TRGO/NR nanocomposites

Fig. 5 shows the variation of the electrical conductivity and dielectric permittivity in the frequency domain with increasing nanofiller content at 25 °C. It is accepted that the electrical properties of nanocomposites depend primarily on the way that the conductive fillers are distributed within the polymer–matrix [31]. The electrical conductivity of TRGO-B nanocomposites (Fig. 5a) gradually increases with increasing filler content, achieving a maximum value of 10^{-4} S/cm at 4 wt.% of TRGO-B. At 2 wt.% filler loading, the conductivity of the TRGO-B nanocomposites is only slightly higher than that of NR, because the filler particles are separated by the insulating rubber matrix. Since the filler is conductive and the matrix is insulating, NR and TRGO-B/NR composites containing 2 wt.% of TRGO present capacitance effects, which are evidenced by the dependence of the electrical conductivity with frequency. However, at low frequencies, an increase in electrical conductivity of about 6 orders of magnitude is observed for nanocomposite containing 3 wt.% nanofiller, indicating that a percolated network has been achieved. The curve corresponding to TRGO-B/NR composites containing 3 wt.% of TRGO-B is also characterized by two zones, an Ohmic or frequency independent zone at low frequencies and a second at higher frequencies where capacitance effects play a role. For higher TRGO-B loadings (4 wt.%) a fairly constant conductivity independent of the frequency is

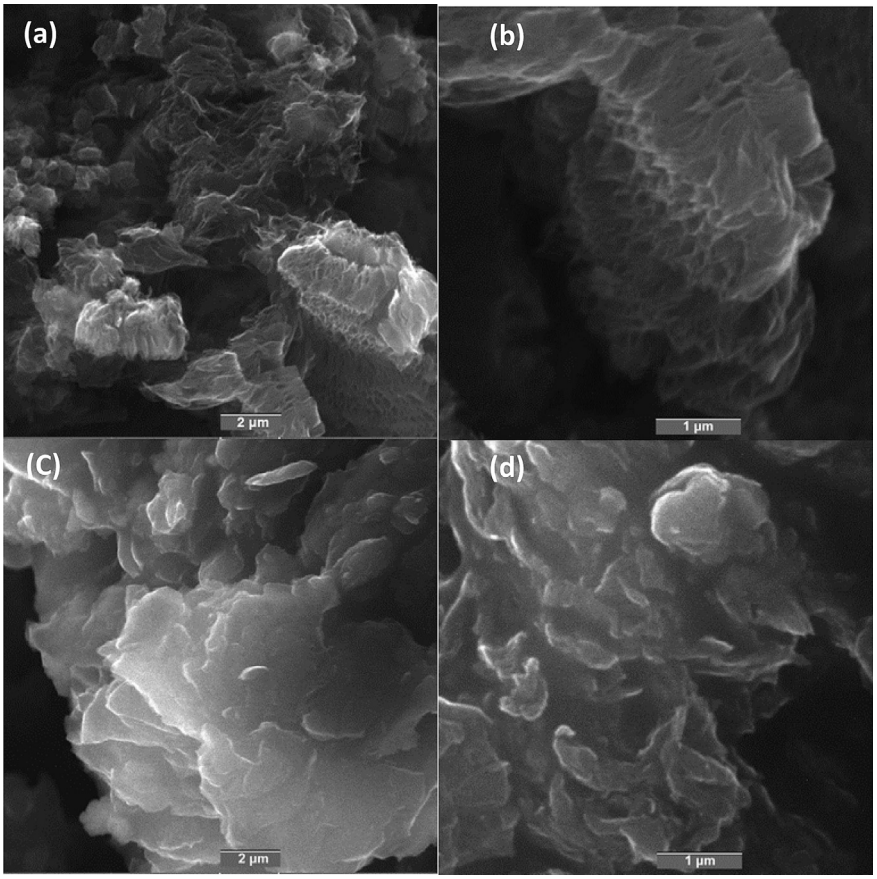

Fig. 3. SEM images of TRGO-B (a and b) and TRGO-H (c and d).

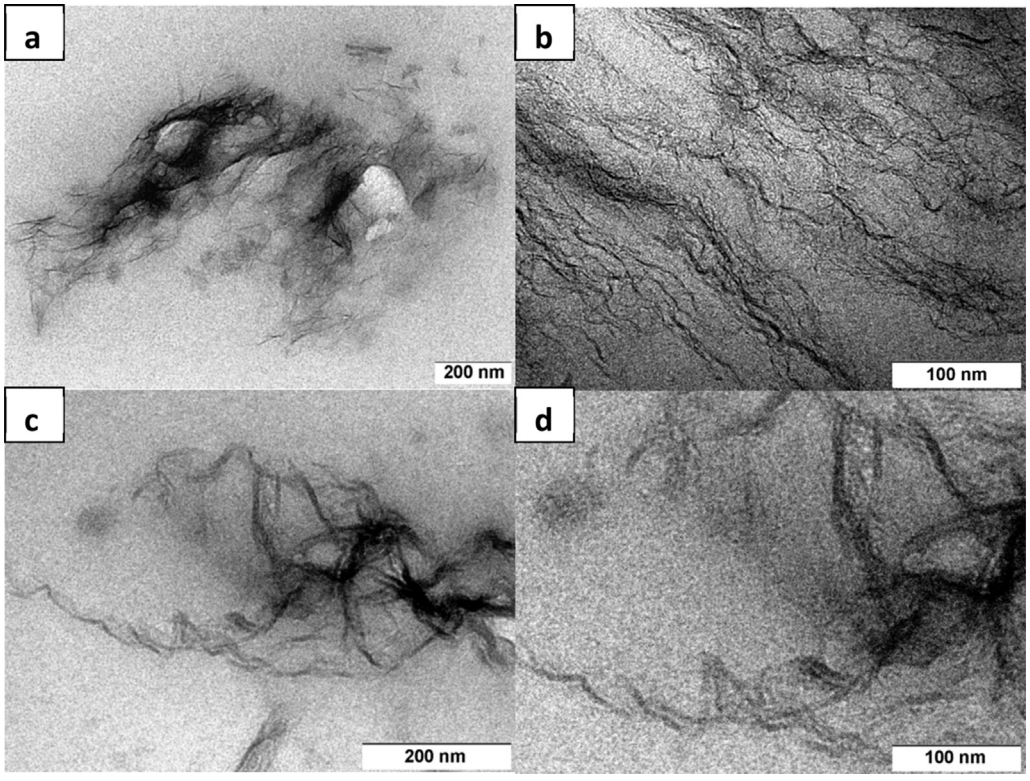

Fig. 4. TEM images of nanocomposites. TRGO-B/NR (a and b) and TRGO-H/NR (c and d).

Table 2
Mechanical properties of TRGO/NR nanocomposites.

Sample	Stress at 100% strain (MPa)	Stress at 300% strain (MPa)	Stress at 500% strain (MPa)	Maximum Stress (MPa)	Deformation at break (%)
NR	0.49 ± 0.01	0.83 ± 0.02	1.39 ± 0.10	14.0 ± 1.01	892 ± 61
DTAB (4.6 wt. %)/NR	0.39 ± 0.01	0.62 ± 0.01	0.94 ± 0.01	10.9 ± 0.58	1044 ± 74
DTAB (6.9 wt. %)/NR	0.38 ± 0.01	0.58 ± 0.02	0.97 ± 0.02	9.69 ± 0.37	958 ± 72
DTAB (9.3 wt.%)/NR	0.36 ± 0.01	0.57 ± 0.01	0.90 ± 0.04	9.16 ± 0.38	962 ± 53
DTAB (4.6 wt. %)/TRGO-B (2 wt.%)/NR	0.57 ± 0.02	1.20 ± 0.06	3.12 ± 0.48	13.1 ± 0.64	778 ± 31
DTAB (6.9 wt. %)/TRGO-B (3 wt.%)/NR	0.65 ± 0.01	1.28 ± 0.02	3.02 ± 0.07	15.1 ± 1.04	806 ± 23
DTAB (9.3 wt.%)/TRGO-B (4 wt.%)/NR	0.65 ± 0.03	1.32 ± 0.03	3.22 ± 0.06	12.0 ± 0.87	751 ± 41
DTAB (4.6 wt. %)/TRGO-H (2 wt.%)/NR	0.44 ± 0.01	0.72 ± 0.01	1.31 ± 0.04	12.0 ± 0.01	877 ± 39
DTAB (6.9 wt. %)/TRGO-H (3 wt.%)/NR	0.42 ± 0.02	0.72 ± 0.03	1.48 ± 0.02	10.3 ± 0.04	867 ± 14
DTAB (9.3 wt.%)/TRGO-H (4 wt.%)/NR	0.43 ± 0.02	0.75 ± 0.02	1.64 ± 0.06	9.63 ± 0.34	853 ± 14

observed, evidencing that the electrically percolation threshold is densified beyond percolation, with contacting fillers and hence presenting an Ohmic behavior.

This information is complemented by the dielectric permittivity (Fig. 5b), which presents curves with a negative slope for 4 and 3 wt.% filler loading. This behavior suggests an effect associated to the Maxwell–Wagner–Sillars effect for heterophasic systems, consisting in interface polarization of insulating polymer/conductive filler systems [44–46]. On the other hand, the NR nanocomposites based on TRGO-H (Fig. 5c and d) do not present significant changes in electrical conductivity or dielectric permittivity, which indicates that the percolation threshold is not reached. This is again correlated with the morphology of the TRGO-H (Fig. 3c and d), which presents small aggregates with low interconnection among the TRGO-H layers. On the contrary, the exfoliated stacking galleries provided by the Brodie's method seem to provide more opportunity for electron transfer among overlapping π-bonds in TRGO. Hence, the morphology of TRGO plays a key role in the formation of the percolation network and consequently in the resulting electrical properties of NR nanocomposites.

4. Conclusions

Thermally reduced graphite oxides (TRGO) were produced from thermal reduction of graphite oxide prepared by two methods previously reported by Brodie and Hummers. Important morphological differences were observed for TRGOs synthesized by those two different graphite oxidation processes. X-ray diffraction and Raman spectroscopy analyses showed that both TRGOs had similar diffraction patterns and comparable structural ordering. However, TEM investigations revealed that the morphology of the TRGO synthesized by the Brodie's method (TRGO-B) is comprised

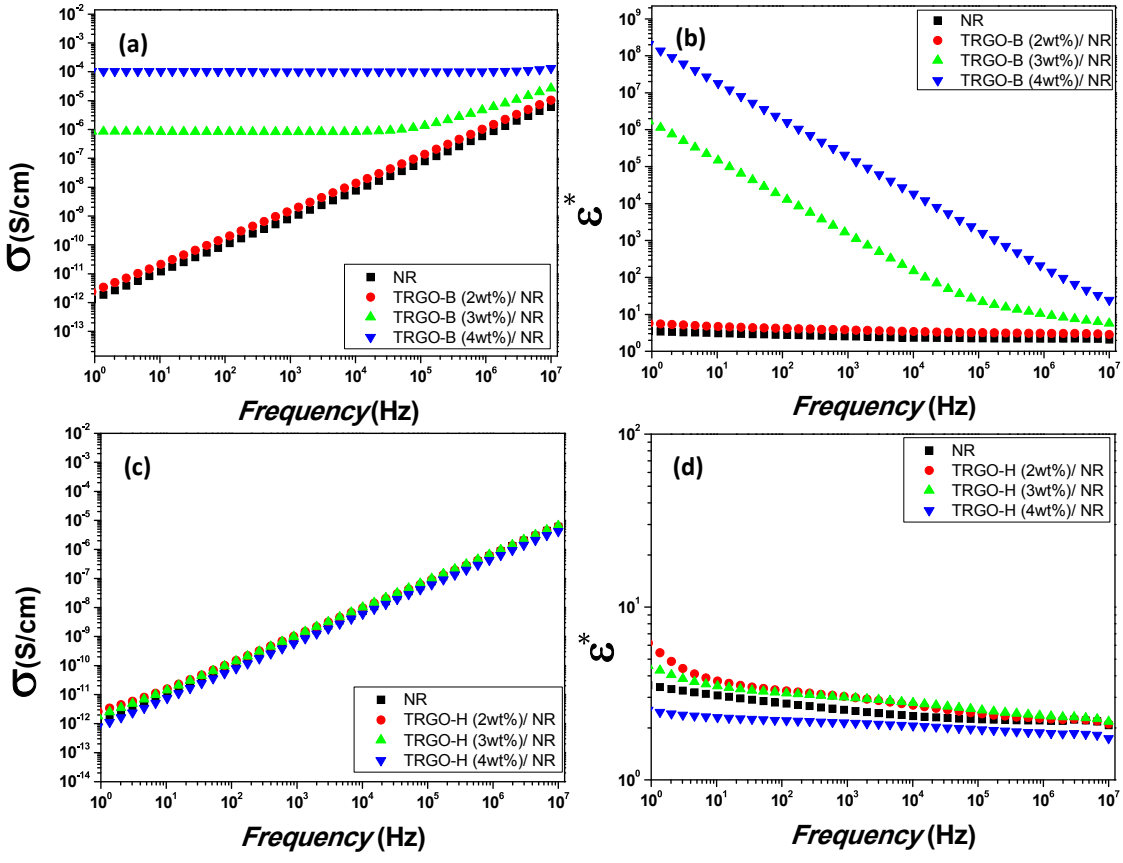

Fig. 5. Dielectric spectroscopy of NR, TRGO-B/NR and TRGO-H/NR nanocomposites.

partially exfoliated stacked galleries, while TRGO produced by the Hummer's method (TRGO-H) showed randomly oriented layers, which seems to be less interconnected. TRGO-B also showed a more homogeneous dispersion and distribution through the natural rubber matrix, contributing to the improvement of the stiffness and particularly the electrical properties of these nanocomposites. TRGO-B/NR nanocomposites showed higher AC electrical conductivity compared to TRGO-H/NR nanocomposites, reaching electrical percolation at TRGO-B concentrations between 2 and 3 wt.%. The maximum conductivity reached by using TRGO-B as nanofiller was of the order of 10^{-4} S/cm at 4 wt.% nanofiller loading. This fact suggests that the stacked morphology of TRGO-B may promote the electron transfer through delocalized π-electrons. On the other hand, the use of TRGO-H rendered only moderate improvements in stiffness and electrical conductivity of the nanocomposites at 4 wt.% nanofiller loading. The results of this research indicate that the morphology of thermally reduced graphite oxides plays a key role in the formation of a percolated network in natural rubber composites, and hence in the resulting electrical and mechanical properties of the nanocomposite.

Acknowledgments

This research was supported by National Commission for Scientific and Technological Research (CONICYT)-Chile project FONDECYT 1131139, the Spanish Ministry of Science and Innovation (MICINN) – Spain, under Project MAT 2010-1874. Moreover, FA and MYP acknowledge additional support for their collaboration from CONACYT-Mexico, Project CIAM Nº 188089 and CONICYT-Chile, Project Nº 120003.

References

[1] Reich S, Thomsen C. Raman spectroscopy of graphite. Phil Trans R Soc Lond A 1824;2004(362):2271–88.
[2] Allen MJ, Tung VC, Kaner RB. Honeycomb carbon: a review of graphene. Chem Rev 2010;110(1):132–45.
[3] Novoselov KS, Geim AK, Morozov SV, Jiang D, Zhang Y, Dubonos SV, et al. Electric field effect in atomically thin carbon films. Science 2004;306(5696):666–9.
[4] Puangbuppha B, Limsuwan P, Asanithi P. Non-chemically functionalized graphene exfoliated from graphite in water using ultrasonic treatment. Proc Eng 2012;32:1094–9.
[5] Zhu Y, Murali S, Cai W, Li X, Suk JW, Potts JR, et al. Graphene and graphene oxide: synthesis, properties, and applications. Adv Mater 2010;22(35):3906–24.
[6] Sadasivuni KK, Ponnamma D, Thomas S, Grohens Y. Evolution from graphite to graphene elastomer composites. Prog Polym Sci 2013;39(4):749–80.
[7] Brodie BC. On the atomic weight of graphite. Phil Trans R Soc Lond 1859;149:249–59.
[8] Staudenmaier L. Verfahren zur Darstellung der Graphitsäure. Ber Dtsch Chem Ges 1898;31(2):1481–7.
[9] Hummers WS, Offeman RE. Preparation of graphitic oxide. J Am Chem Soc 1958;80(6):1339.
[10] Lenher V, Stone HW, Skinner HH. NOTE. The formation of potassium perchlorate from potassium chlorate. J Am Chem Soc 1922;44(1):143–4.
[11] Koch KR. Oxidation by Mn207: an impressive demonstration of the powerful oxidizing property of dimanganeseheptoxide. J Chem Educ 1982;59(11):973.
[12] Botas C, Álvarez P, Blanco P, Granda M, Blanco C, Santamaría R, et al. Graphene materials with different structures prepared from the same graphite by the Hummers and Brodie methods. Carbon 2013;65:156–64.
[13] Rocha CG, Rümmeli MH, Ibrahim I, Sevincli H, Börrnert F, Kunstmann J, et al. Tailoring the physical properties of graphene. In: Choi J-W, Lee W, editors. Graphene: synthesis and applications. Boca Raton: CRC Press; 2011. p. 1–26.
[14] Stankovich S, Dikin DA, Dommett GHB, Kohlhaas KM, Zimney EJ, Stach EA, et al. Graphene-based composite materials. Nature 2006;442(7100):282–6.
[15] Kim H, Abdala AA, MacOsko CW. Graphene/polymer nanocomposites. Macromolecules 2010;43(16):6515–30.
[16] Du J, Cheng HM. The fabrication, properties, and uses of graphene/polymer composites. Macromol Chem Phys 2012;213(10–11):1060–77.
[17] Young RJ, Kinloch IA, Gong L, Novoselov KS. The mechanics of graphene nanocomposites: a review. Compos Sci Technol 2012;72(12):1459–76.
[18] Verdejo R, Bernal MM, Romasanta LJ, Lopez-Manchado MA. Graphene filled polymer nanocomposites. J Mater Chem 2011;21(10):3301–10.
[19] Malas A, Pal P, Giri S, Mandal A, Das CK. Synthesis and characterizations of modified expanded graphite/emulsion styrene butadiene rubber nanocomposites: mechanical, dynamic mechanical and morphological properties. Compos Part B Eng 2014;58:267–74.
[20] Pokharel P, Pant B, Pokhrel K, Pant HR, J-g Lim, Lee DS, et al. Effects of functional groups on the graphene sheet for improving the thermomechanical properties of polyurethane nanocomposites. Compos Part B Eng 2015;78:192–201.
[21] Gan L, Shang S, Yuen CWM, Jiang S-x, Luo NM. Facile preparation of graphene nanoribbon filled silicone rubber nanocomposite with improved thermal and mechanical properties. Compos Part B Eng 2015;69:237–42.
[22] Malas A, Das CK. Effect of graphene oxide on the physical, mechanical and thermo-mechanical properties of neoprene and chlorosulfonated polyethylene vulcanizates. Compos Part B Eng 2015;79:639–48.
[23] Wang H, Xie G, Fang M, Ying Z, Tong Y, Zeng Y. Electrical and mechanical properties of antistatic PVC films containing multi-layer graphene. Compos Part B Eng 2015;79:444–50.
[24] Hernández M, Bernal MdM, Verdejo R, Ezquerra TA, López-Manchado MA. Overall performance of natural rubber/graphene nanocomposites. Compos Sci Technol 2012;73(0):40–6.
[25] Prud'homme R, Ozbas B, Aksay I, Register R, Adamson D, inventors. Functional graphene rubber nanocomposites. US7745528B2. United States: 2010.
[26] Zhan Y, Wu J, Xia H, Yan N, Fei G, Yuan G. Dispersion and exfoliation of graphene in rubber by an ultrasonically-assisted latex mixing and in situ reduction process. Macromol Mater Eng 2011;296(7):590–602.
[27] Zhan Y, Lavorgna M, Buonocore G, Xia H. Enhancing electrical conductivity of rubber composites by constructing interconnected network of self-assembled graphene with latex mixing. J Mater Chem 2012;22(21):10464–8.
[28] Potts JR, Shankar O, Du L, Ruoff RS. Processing–morphology–property relationships and composite theory analysis of reduced graphene oxide/natural rubber nanocomposites. Macromolecules 2012;45(15):6045–55.
[29] Potts JR, Shankar O, Murali S, Du L, Ruoff RS. Latex and two-roll mill processing of thermally-exfoliated graphite oxide/natural rubber nanocomposites. Compos Sci Technol 2013;74(0):166–72.
[30] Tian M, Zhang J, Zhang L, Liu S, Zan X, Nishi T, et al. Graphene encapsulated rubber latex composites with high dielectric constant, low dielectric loss and low percolation threshold. J Colloid Interface Sci 2014;430:249–56.
[31] Aguilar-Bolados H, Brasero J, Lopez-Manchado MA, Yazdani-Pedram M. High performance natural rubber/thermally reduced graphite oxide nanocomposites by latex technology. Compos Part B Eng 2014;67:449–54.
[32] Xing W, Wu J, Huang G, Li H, Tang M, Fu X. Enhanced mechanical properties of graphene/natural rubber nanocomposites at low content. Polym Int 2014;63(9):1674–81.
[33] Matos CF, Galembeck F, Zarbin AJG. Multifunctional and environmentally friendly nanocomposites between natural rubber and graphene or graphene oxide. Carbon 2014;78:469–79.
[34] Test methods for vulcanized rubber and thermoplastic elastomers–tension. ASTM International; 2008.
[35] Marcano DC, Kosynkin DV, Berlin JM, Sinitskii A, Sun Z, Slesarev A, et al. Improved synthesis of graphene oxide. ACS Nano 2010;4(8):4806–14.
[36] Botas C, Álvarez P, Blanco C, Santamaría R, Granda M, Gutiérrez MD, et al. Critical temperatures in the synthesis of graphene-like materials by thermal exfoliation–reduction of graphite oxide. Carbon 2013;52:476–85.
[37] Ferrari AC, Basko DM. Raman spectroscopy as a versatile tool for studying the properties of graphene. Nat Nanotechnol 2013;8(4):235–46.
[38] Saito R, Hofmann M, Dresselhaus G, Jorio A, Dresselhaus MS. Raman spectroscopy of graphene and carbon nanotubes. Adv Phys 2011;60(3):413–550.
[39] Lucchese MM, Stavale F, Ferreira EHM, Vilani C, Moutinho MVO, Capaz RB, et al. Quantifying ion-induced defects and Raman relaxation length in graphene. Carbon 2010;48(5):1592–7.
[40] Cancado LG, Jorio A, Ferreira EHM, Stavale F, Achete CA, Capaz RB, et al. Quantifying defects in graphene via Raman spectroscopy at different excitation energies. Nano Lett 2011;11(8):3190–6.
[41] Chabot V, Kim B, Sloper B, Tzoganakis C, Yu A. High yield production and purification of few layer graphene by gum arabic assisted physical sonication. Sci Rep 2013;3:1–7.
[42] Ferrari AC, Meyer JC, Scardaci V, Casiraghi C, Lazzeri M, Mauri F, et al. Raman spectrum of graphene and graphene layers. Phys Rev Lett 2006;97(18):187401.
[43] Steward PA, Hearn J, Wilkinson MC. An overview of polymer latex film formation and properties. Adv Colloid Interface Sci 2000;86(3):195–267.
[44] Hayward D, Pethrick RA, Siriwittayakorn T. Dielectric studies of heterogeneous phase polymer systems: poly(ethylene oxide) inclusions in polycarbonate - a model system. Macromolecules 1992;25(5):1480–6.
[45] Pelster R, Simon U. Nanodispersions of conducting particles: preparation, microstructure and dielectric properties. Colloid Polym Sci 1999;277(1):2–14.
[46] Martin-Gallego M, Hernández M, Lorenzo V, Verdejo R, Lopez-Manchado MA, Sangermano M. Cationic photocured epoxy nanocomposites filled with different carbon fillers. Polymer 2012;53(9):1831–8.